Genus Zero Surface Conformal Mapping and Its Application to Brain Surface Mapping

Xianfeng Gu, Yalin Wang*, Tony F. Chan, Paul M. Thompson, and Shing-Tung Yau

***Abstract*—We developed a general method for global conformal parameterizations based on the structure of the cohomology group of holomorphic one-forms for surfaces with or without boundaries (Gu and Yau, 2002), (Gu and Yau, 2003). For genus zero surfaces, our algorithm can find a unique mapping between any two genus zero manifolds by minimizing the harmonic energy of the map. In this paper, we apply the algorithm to the cortical surface matching problem. We use a mesh structure to represent the brain surface. Further constraints are added to ensure that the conformal map is unique. Empirical tests on magnetic resonance imaging (MRI) data show that the mappings preserve angular relationships, are stable in MRIs acquired at different times, and are robust to differences in data triangulation, and resolution. Compared with other brain surface conformal mapping algorithms, our algorithm is more stable and has good extensibility.**

***Index Terms*—Brain mapping, conformal map, landmark matching, spherical harmonic transformation.**

I. Introduction

RECENT developments in brain imaging have accelerated the collection and databasing of brain maps. Nonetheless, computational problems arise when integrating and comparing brain data. One way to analyze and compare brain data is to map them into a canonical space while retaining geometric information on the original structures as far as possible [3]–[9]. Among them, Schwartz *et al.* [3] and Timsari [7] computed quasi-isometric flat maps of the cerebral cortex. Hurdal *et al.* [5] and Haker *et al.* [6] computed quasi-conformal and conformal maps of the cerebral cortex, respectively.

A. Previous Work

Conformal surface parameterizations have been studied intensively. Most works on conformal parameterizations deal with surface patches homeomorphic to topological disks. For surfaces with arbitrary topologies, Gu and Yau [1] introduce a general conformal parameterization based on a nonlinear flow for the genus zero case, and on the structure of the cohomology group of holomorphic one-forms in the case of genus greater than one. They generalize the method for surfaces with boundaries in [2]. In this paper, we apply part of these algorithms (for the genus zero case) to the cortical surface matching problem and report our experimental results. In particular, the algorithms used in Sections II, III, and IV, are from [1], [2] and the data compression using spherical harmonic was also conceived there for other purposes.

It is well known that all orientable surfaces are Riemann surfaces. If two surfaces can be conformally mapped to each other, they share the same conformal structure. Therefore, computing conformal mappings is equivalent to computing conformal structures for surfaces. For genus zero closed surfaces, harmonic maps are equivalent to conformal maps [10]. Many algorithms for surface parameterization are based on harmonic maps. By adding a periodic boundary condition, the harmonic mapping method can be generalized for the genus one case. For the higher genus case, the method is not applicable any more.

1) Conformal Parameterization for Genus Zero Surfaces: Most works on conformal parameterization only deal with genus zero surfaces. There are five basic approaches to achieve conformal parameterizations.

a) *Harmonic energy minimization*. Eck *et al.* [11] introduce the discrete harmonic map, which approximates the continuous harmonic map [10] by minimizing a *metric dispersion* criterion. Desbrun *et al.* [12], [13] compute the discrete Dirichlet energy and apply conformal parameterization for interactive geometry remeshing. Pinkall and Polthier compute the discrete harmonic map and Hodge star operator for the purpose of creating a minimal surface [14]. Kanai *et al.* use a harmonic map for geometric metamorphosis in [15]. While the discrete harmonic mapping is used, it is not clear that it approximates the harmonic map defined in the smooth category. Gu and Yau in [1] introduce a nonlinear optimization method to compute global conformal parameterizations for genus zero surfaces. The optimization is carried out in the tangent spaces of the sphere. It is different from the previous optimization methods. It computes global parameterizations for genus zero surfaces.

b) *Cauchy–Riemann equation approximation*. Levy *et al.* [16] compute a quasi-conformal parameterization of topological disks by approximating the Cauchy–Riemann

Manuscript received January 5, 2004; revised April 28, 2004. This paper is an extended version of a paper published in *Lecture Notes in Computer Science (Proceedings of Information Processing in Medical Imaging)*, 2003 [32]. This work was supported in part by the National Institutes of Health (NIH) under Grant R21 EB001 561 and Grant R21 RR019 771; in part by the National Science Foundation (NSF) under Contract DMS-9973341, NSF Contract ACI-0072112, ONR Contract N00014-03-1-0888, and NIH Contract P20 MH65166. The Guest Editors responsible for coordinating the review of this paper and recommending its publication were C. J. Taylor and J. A. Noble. *Asterisk indicates corresponding author*.

X. Gu is with the Department of Computer and Information Science and Engineering, University of Florida, FL 32611 USA (e-mail: gu@cise.ufl.edu).

*Y. Wang is with the Mathematics Department, the University of California, Los Angeles, CA 90095 USA (e-mail: ylwang@math.ucla.edu).

T. F. Chan is with the Mathematics Department, the University of California, Los Angeles, CA 90095 USA (e-mail: chan@math.ucla.edu).

P. M. Thompson is with the Laboratory of Neuro Imaging, Department of Neurology, School of Medicine, the University of California, Los Angeles USA (e-mail: thompson@loni.ucla.edu).

S.-T. Yau is with the Department of Mathematics, Harvard University, Cambridge, MA 02138 USA (e-mail: yau@math.harvard.edu).

Digital Object Identifier 10.1109/TMI.2004.831226

TABLE I
APPROACHES FOR CONFORMAL AND HARMONIC SURFACE PARAMETERIZATION

Method	*Principle*	*Comments*
Discrete Harmonic Maps [11]–[14]	Minimize harmonic energy, namely the Dirichlet energy	Compute harmonic maps for genus zero surfaces only
Least-square Conformal Mapping [16]	Approximate Cauchy-Riemann equation	Equivalent to harmonic energy
Laplace-Beltrami operator [17], [20]	A linear system which approximates the Laplace-Beltrami operator	Compute conformal maps for closed genus zero and genus one surfaces
Angle-Based Functional [18]	Minimizes distortion in angle space	Computes conformal maps for closed genus zero and genus one surfaces
Circle Packing [19], [21]	Based on mean value property of harmonic maps	Does not consider the specific metric
Conformal Structure [1], [2]	Compute cohomology group of holomorphic 1-forms	Based on Hodge theory, general approach for arbitrary genus surfaces

equation using the least squares method. They show rigorously that the quasi-conformal parameterization exists uniquely, and is invariant to similarity transformations, independent of resolution, and orientation-preserving.

c) *Laplacian operator linearization*. Haker *et al.* [6], [17] use a method to compute a global conformal mapping from a genus zero surface to a sphere by representing the Laplace–Beltrami operator as a linear system.

d) *Angle-based method*. Sheffer *et al.* [18] introduce an angle-based flattening method to flatten a mesh to a two-dimensional plane so that it minimizes the relative distortion of the planar angles with respect to their counterparts in the three-dimensional (3-D) space.

e) *Circle packing*. Circle packing is introduced in [5], [19]. Classical analytic functions can be approximated using circle packing. For general surfaces in $\mathbb{R}^3$, the circle packing method considers only the connectivity but not the geometry, so it is not suitable for our parameterization purpose.

2) Global Conformal Parameterization for Nonzero Genus Closed Surfaces: For genus one surfaces, conformal parameterization is introduced in [20] by adding periodic constraints for harmonic maps defined on the fundamental domain of the surface.

It is impossible to generalize the current harmonic mapping method to the high genus case. The problem of computing conformal structures for general surfaces with arbitrary topologies is completely solved by Gu and Yau in [1], [2]. The method is based on Hodge theory, and applicable for both closed surfaces and open surfaces with arbitrary genus.

We summarize current conformal and harmonic surface parameterization methods in Table I.

There are some methods applying the Möbius automorphism group to brain conformal mapping. For instance, Tosun *et al.* [22], [23] used an approach based on Haker's conformal mapping and employed a Möbius transformation to minimize area distortion and sulcal alignment across multiple brains.

B. Basic Idea

Suppose M_1, M_2 are two surfaces. Locally they can be represented as $r_1(x^1, x^2), r_2(x^1, x^2)$, where (x^1, x^2) are their local coordinates, and $r_1, r_2 : R^2 \to R^3$ are vector-valued functions. The first fundamental form of M_1 is $ds_1^2 = \sum_{ij} g_{ij} dx^i dx^j$, where

$$g_{ij} = \frac{\partial r_1}{\partial x^i} \cdot \frac{\partial r_1}{\partial x^j}, \quad i, j = 1, 2$$

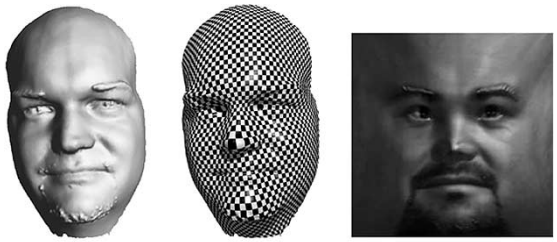

Fig. 1. Conformal surface parameterization examples. (a) Is a real male face. (c) Is a square into which the human face is conformally mapped. (b) Is the conformal parameterization illustrated by the texture map. As shown, the right angles on the checkboard are well preserved on the surface in (b).

Similarly, the first fundamental form of M_2 is defined in the same way. $ds_2^2 = \sum_{ij} \tilde{g}_{ij} dx^i dx^j$. Define a mapping $f : M_1 \to M_2$ between two surfaces. Using local coordinates, f can be represented as $f : R^2 \to R^2, f = (f^1(x^1, x^2), f^2(x^1, x^2))$. Then any tangent vector (dx^1, dx^2) on M_1 will be mapped to a tangent vector df on M_2

$$\begin{pmatrix} df^1 \\ df^2 \end{pmatrix} = \begin{pmatrix} \frac{\partial f^1}{\partial x_1} & \frac{\partial f^1}{\partial x_2} \\ \frac{\partial f^2}{\partial x_1} & \frac{\partial f^2}{\partial x_2} \end{pmatrix} \begin{pmatrix} dx^1 \\ dx^2 \end{pmatrix}. \tag{1}$$

The length of df is

$$\sum_{m,n} \tilde{g}_{mn} df^m df^n. \tag{2}$$

We use the length of df to define the length of (dx^1, dx^2). Namely, we define a new metric for M_1 which is induced by the mapping f and the metric on M_2. We call this metric *the pull-back metric*, and denote it by $f^* ds_2^2$. Replacing df^m in (2) by (1), we get the analytic formula for the pull-back metric

$$f^* ds_2^2 = \sum_{mn} \left(\sum_{ij} \tilde{g}_{ij}(f(x^1, x^2)) \frac{\partial f^m}{\partial x_i} \frac{\partial f^n}{\partial x_j} \right) dx^m \, dx^n. \tag{3}$$

We call f a *conformal mapping*, if there exists a positive scalar function $\lambda(x^1, x^2)$, such that

$$f^* ds_2^2 = \lambda(x^1, x^2) \, ds_1^2 \tag{4}$$

where $\lambda(x^1, x^2)$ is called the *conformal factor*.

Intuitively, all the angles on M_1 are preserved on M_2. Fig. 1 shows a conformal mapping example. Fig. 1(a) shows a real male face. We conformally map it to a square as in 1(c) and get its conformal parameterization. We illustrate the conformal parameterization via the texture mapping of a checkerboard in Fig. 1.

It is well known that any genus zero surface can be mapped conformally onto the sphere and any local portion thereof onto a disk. This mapping, a conformal equivalence, is one-to-one, onto, and angle-preserving. Moreover, the elements of the first fundamental form remain unchanged, except for a scaling factor (the so-called *Conformal Factor*). For this reason, conformal mappings are often described as being similarities in the small. Since the cortical surface of the brain is a genus zero surface, conformal mapping offers a convenient method to retain local geometric information, when mapping data between surfaces. Indeed, several groups have created flattened representations or visualizations of the cerebral cortex or cerebellum [5], [6] using conformal mapping techniques. However, these approaches are either not strictly angle preserving [5], or there may be areas with large geometric distortions [6]. In this paper, we propose a new genus zero surface conformal mapping algorithm [1] and demonstrate its use in computing conformal mappings between brain surfaces. Our algorithm depends only on the surface geometry and is invariant to changes in image resolution and the specifics of the data triangulation. Our experimental results show that our algorithm has advantageous properties for cortical surface matching.

Suppose K is a simplicial complex, and $f\colon |K| \to R^3$, which embeds $|K|$ in R^3; then (K, f) is called a mesh. Given two genus zero meshes M_1, M_2, there are many conformal mappings between them. Our algorithm for computing conformal mappings is based on the fact that for genus zero surfaces $S_1, S_2, f : S_1 \to S_2$ is conformal if and only if f is harmonic. All conformal mappings between S_1, S_2 form a group, the so-called Möbius group. Fig. 2 shows some examples of Möbius transformations. We can conformally map the surface of the head of Michelangelo's David to a sphere. When we draw the longitude and latitude lines on the sphere, we can induce corresponding circles on the original surface [Fig. 2(a) and (b)]. We apply a Möbius transformation to the sphere and make the two eyes become north and south poles. When we draw the longitude and latitude lines again [Fig. 2(c)], we get an interesting result shown in Fig. 2(d). Note all the right angles between the lines are well preserved in Fig. 2(b) and (d). This example demonstrates that all the conformal mapping results form a Möbius group.

Our method is summarized as follows: we first find a homeomorphism h between M_1 and M_2, then deform h such that h minimizes the harmonic energy. To ensure the convergence of the algorithm, constraints are added; this also ensures that there is a unique conformal map.

This paper is organized as follows. In Section II, we give the definitions of a piecewise linear function space, inner product and piecewise Laplacian. In Section III, we describe the steepest descent algorithm which is used to minimize the string energy. In Section IV, we detail our conformal spherical mapping algorithms. In Section V, the conformal parameterization is optimized by integrating landmark information. Section VI applies conformal mapping for spherical harmonic transformation, and rotation-invariant shape analysis. Experimental results on conformal mapping for brain surfaces are reported in Section VII. In Section VIII, we compare our algorithm with other conformal mapping approaches used in neuroimaging. We conclude the paper in Section IX.

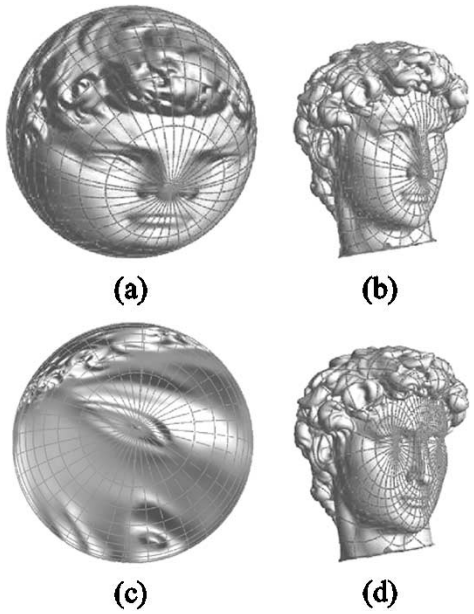

Fig. 2. Möbius transformation example. We conformally map the surface of the head of Michelangelo's David to a sphere. In (a), we select the nose tip as the north pole and draw longitude and latitude lines on the sphere. (b) Shows the results on the original David head model. We apply a Möbius transformation on the sphere in (a) and make the two eyes become the north and south poles. When drawing the longitude and latitude lines on the sphere (c), we get an interesting configuration for the lines on the original surface (d).

II. Piecewise Linear Function Space, Inner Product and Laplacian

If a diffeomorphism between genus zero surfaces minimizing the harmonic energy, it is conformal. Based on this fact, the algorithm is designed as a steepest descent method.

This section formulates the mathematical concepts in a rigorous way. The major concepts, the harmonic energy of a map and its derivative, are defined. Because all the calculation is carried out on surfaces, we use the absolute derivative. Furthermore, for the purpose of implementation, we introduce the definitions in discrete form.

We use K to represent the simplicial complex, u, v to denote the vertices, and $\{u, v\}$ to denote the edge spanned by u, v. We use f, g to represent the piecewise linear functions defined on K, use $\vec{f}$ to represent vector value functions. We use Δ_{PL} to represent the discrete Laplacian operator.

Definition 1: All piecewise linear functions defined on K form a linear space, denoted by $C^{\mathrm{PL}}(K)$.

In practice, we use $C^{\mathrm{PL}}(K)$ to approximate all functions defined on K. So the final result is an approximation to the conformal mapping. The higher the resolution of the mesh is, the more accurate the approximated conformal mapping is.

Definition 2: Suppose a set of string constants $k_{u,v}$ are assigned for each edge $\{u, v\}$, the inner product on C^{PL} is defined as the quadratic form

$$\langle f, g\rangle = \frac{1}{2} \sum_{\{u,v\}\in K} k_{u,v}(f(u) - f(v))(g(u) - g(v)). \quad (5)$$

The energy is defined as the norm on C^{PL}.

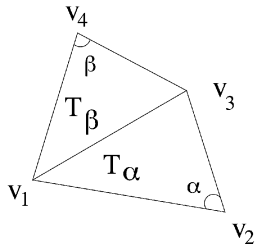

Fig. 3. Discrete Laplace–Beltrami operator. Edge $\{v_1, v_3\}$ has two corners against it α, β. The edge weight is defined as the summation of the cotangents of these corner angles.

Definition 3: Suppose $f \in C^{\mathrm{PL}}$, the string energy is defined as:

$$E(f) = \langle f, f \rangle = \sum_{\{u,v\} \in K} k_{u,v} \|f(u) - f(v)\|^2. \tag{6}$$

By changing the string constants $k_{u,v}$ in the energy formula, we can define different string energies.

Definition 4: If string constants $k_{u,v} \equiv 1$, the string energy is known as the Tuette energy.

Definition 5: Suppose edge $\{u, v\}$ has two adjacent faces T_α, T_β, with $T_\alpha = \{v_1, v_2, v_3\}$, as shown in Fig. 3, define the parameters

$$a^{\alpha}_{v_1,v_2} = \frac{1}{2} \frac{(v_1 - v_3) \cdot (v_2 - v_3)}{|(v_1 - v_3) \times (v_2 - v_3)|} \tag{7}$$

$$a^{\alpha}_{v_2,v_3} = \frac{1}{2} \frac{(v_2 - v_1) \cdot (v_3 - v_1)}{|(v_2 - v_1) \times (v_3 - v_1)|} \tag{8}$$

$$a^{\alpha}_{v_3,v_1} = \frac{1}{2} \frac{(v_3 - v_2) \cdot (v_1 - v_2)}{|(v_3 - v_2) \times (v_1 - v_2)|} \tag{9}$$

T_β is defined similarly. If $k_{u,v} = a^{\alpha}_{u,v} + a^{\beta}_{u,v}$, the string energy obtained is called the *harmonic energy*.

The string energy is always a quadratic form. By carefully choosing the string coefficients, we make sure the quadratic form is positive definite. This will guarantee the convergence of the steepest descent method.

Definition 6: The piecewise Laplacian is the linear operator Δ_{PL}: $C^{\mathrm{PL}} \to C^{\mathrm{PL}}$ on the space of piecewise linear functions on K, defined by the formula

$$\Delta_{\mathrm{PL}}(f) = \sum_{\{u,v\} \in K} k_{u,v}(f(v) - f(u)). \tag{10}$$

If f minimizes the string energy, then f satisfies the condition $\Delta_{\mathrm{PL}}(f) = 0$. Suppose M_1, M_2 are two meshes and the map $\vec{f}$: $M_1 \to M_2$ is a map between them, $\vec{f}$ can be treated as a map from M_1 to R^3 also.

Definition 7: For a map $\vec{f} : M_1 \to R^3, \vec{f} = (f_0, f_1, f_2), f_i \in C^{\mathrm{PL}}, i = 0, 1, 2$, we define the energy as the norm of $\vec{f}$

$$E(\vec{f}) = \sum_{i=0}^{2} E(f_i). \tag{11}$$

The Laplacian is defined in a similar way.

Definition 8: For a map $\vec{f}$: $M_1 \to R^3$, the piecewise Laplacian of $\vec{f}$ is

$$\Delta_{\mathrm{PL}} \vec{f} = (\Delta_{\mathrm{PL}} f_0, \Delta_{\mathrm{PL}} f_1, \Delta_{\mathrm{PL}} f_2). \tag{12}$$

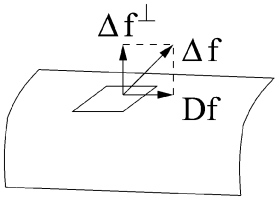

Fig. 4. Projected Laplacian. The Laplacian Δf is a vector in R^3, which can be decomposed into a normal component, $(\Delta_{\mathrm{PL}} \vec{f})^{\perp}$, and tangential component, $D\vec{f}$. The normal component is collinear with the normal to the target surface, and the tangential component is in the tangent space of the target surface.

A map $\vec{f} : M_1 \to M_2$ is harmonic, if and only if $\Delta_{\mathrm{PL}} \vec{f}$ only has a normal component, and its tangential component is zero

$$\Delta_{\mathrm{PL}}(\vec{f}) = (\Delta_{\mathrm{PL}} \vec{f})^{\perp}. \tag{13}$$

A decomposition of Laplacian Δf is shown in Fig. 4.

III. Steepest Descent Algorithm

Suppose we would like to compute a mapping $\vec{f} : M_1 \to M_2$ such that $\vec{f}$ minimizes a string energy $E(\vec{f})$. This can be solved easily by the steepest descent algorithm

$$\frac{d\vec{f}(t)}{dt} = -\Delta \vec{f}(t) \tag{14}$$

$\vec{f}(M_1)$ is constrained to be on M_2, so $-\Delta \vec{f}$ is a tangent vector field of M_2.

Specifically, suppose $\vec{f} : M_1 \to M_2$, and denote the image of each vertex $v \in K_1$ as $\vec{f}(v)$. The normal on M_2 at $\vec{f}(v)$ is $\vec{n}(\vec{f}(v))$. Define the normal component as below.

Definition 9: The normal component

$$(\Delta \vec{f}(v))^{\perp} = \langle \Delta \vec{f}(v), \vec{n}(\vec{f}(v)) \rangle \vec{n}(\vec{f}(v)) \tag{15}$$

where $\langle , \rangle$ is the inner product in R^3.

Definition 10: The absolute derivative is defined as

$$D\vec{f}(v) = \Delta \vec{f}(v) - (\Delta \vec{f}(v))^{\perp}. \tag{16}$$

Then, (14) is $\delta \vec{f} = -D\vec{f} \times \delta t$.

IV. Conformal Spherical Mapping

Suppose M_2 is S^2, then a conformal mapping $\vec{f}$: $M_1 \to S^2$ can be constructed by using the steepest descent method. The major difficulty is that the solution is not unique but forms a Möbius group.

Definition 11: Mapping $f : \mathcal{C} \to \mathcal{C}$ is a Möbius transformation if and only if

$$f(z) = \frac{az + b}{cz + d}, \quad a, b, c, d \in \mathcal{C}, \quad ad - bc = 1.0 \tag{17}$$

where $\mathcal{C}$ is the complex plane.

All Möbius transformations form the Möbius transformation group. In order to determine a unique solution we can add different constraints. In practice we use the following two constraints: the zero mass-center constraint and a landmark constraint.

Definition 12: Mapping $\vec{f} : M_1 \to M_2$ satisfies the zero mass-center condition if and only if

$$\int_{M_1} \vec{f} d\sigma_{M_1} = 0 \tag{18}$$

where $d\sigma_{M_1}$ is the area element on M_1.

All conformal maps from M_1 to S^2 satisfying the zero mass-center constraint are unique up to the Euclidean rotation group (which is 3-D). We use the Gauss map as the initial condition.

Definition 13: A Gauss map $N : M_1 \to S^2$ is defined as

$$N(v) = \vec{n}(v), \quad v \in M_1 \tag{19}$$

where $\vec{n}(v)$ is the normal at v.

Algorithm 1: Spherical Tuette Mapping: Input (mesh M, step length δt, energy difference threshold δE), output ($\vec{t} : M \to S^2$) where $\vec{t}$ minimizes the Tuette energy.

1) Compute Gauss map $N : M \to S^2$. Let $\vec{t} = N$, compute Tuette energy E_0.
2) For each vertex $v \in M$, compute absolute derivative $D\vec{t}$.
3) Update $\vec{t}(v)$ by $\delta\vec{t}(v) = -D\vec{t}(v)\delta t$.
4) Compute Tuette energy E.
5) If $|E - E_0| < \delta E$, return $\vec{t}$. Otherwise, assign E to E_0 and repeat steps 2)–5).

Because the Tuette energy has a unique minimum, the algorithm converges rapidly and is stable. We use it as the initial condition for the conformal mapping.

Algorithm 2: Spherical Conformal Mapping: Input (mesh M, step length δt, energy difference threshold δE), output ($\vec{h} : M \to S^2$). Here $\vec{h}$ minimizes the harmonic energy and satisfies the zero mass-center constraint.

1) Compute Tuette embedding $\vec{t}$. Let $\vec{h} = \vec{t}$, compute Tuette energy E_0.
2) For each vertex $v \in M$, compute the absolute derivative $D\vec{h}$.
3) Update $\vec{h}(v)$ by $\delta\vec{h}(v) = -D\vec{h}(v)\delta t$.
4) Compute Möbius transformation $\vec{\varphi}_0 : S^2 \to S^2$, such that

$$\Gamma(\vec{\varphi}) = \int_{M_1} \vec{\varphi} \circ \vec{h} d\sigma_{M_1}, \vec{\varphi} \in M\,\mathrm{obius}(S^2) \tag{20}$$

$$\vec{\varphi}_0 = \min_{\vec{\varphi}} \|\Gamma(\vec{\varphi})\|^2 \tag{21}$$

where $d\sigma_{M_1}$ is the area element on M_1. $\Gamma(\vec{\varphi})$ is the mass center, and $\vec{\varphi}$ minimizes the norm in the mass center condition. $M\,\mathrm{obius}(S^2)$ is the conformal automorphism group of S^2, and it can be analytically represented as $\tau^{-1} \circ \theta \circ \tau$, where $\tau : S^2 \to C$ is the *stereographic projection*

$$\tau(p) = \left(\frac{x}{1-z}, \frac{y}{1-z}\right), \quad p = (x, y, z) \in S^2$$

and $\theta : C \to C$ is a Möbius transformation as defined in Definition 11.

5) compute the harmonic energy E.
6) If $|E - E_0| < \delta E$, return $\vec{t}$. Otherwise, assign E to E_0 and repeat Step 2) through to Step 6).

Step 4) is nonlinear and expensive to compute. In practice we use the following procedure to replace it:

$4'-1)$ compute the mass center $\vec{c} = \int_{S^2} \vec{h} d\sigma_{M_1}$;
$4'-2)$ for all $v \in M, \vec{h}(v) = \vec{h}(v) - \vec{c}$;
$4'-3)$ for all $v \in M, \vec{h}(v) = (\vec{h}(v))/(\|\vec{h}(v)\|)$.

This approximation method is good enough for our purpose. The resulting angle distortion is proportional to the square of the distance between the mass center and the origin. When the deviation is small, this provides a very accurate approximation to a Möbius transformation. By choosing the step length carefully, the energy can be decreased monotonically at each iteration.

V. Optimize the Conformal Parameterization by Using Landmarks

In order to compare two brain surfaces, it is desirable to adjust the conformal parameterization and match the geometric features on the brains as well as possible. We define an energy to measure the quality of the parameterization. Suppose two brain surfaces S_1, S_2 are given, conformal parameterizations are denoted as $f_1 : S^2 \to S_1$ and $f_2 : S^2 \to S_2$, the *matching energy* is defined as

$$E(f_1, f_2) = \int_{S^2} \|f_1(u, v) - f_2(u, v)\|^2 \, du \, dv \tag{22}$$

We can compose a Möbius transformation τ with f_2, such that

$$E(f_1, f_2 \circ \tau) = \min_{\zeta \in \Omega} E(f_1, f_2 \circ \zeta) \tag{23}$$

where Ω is the group of Möbius transformations. We use landmarks to obtain the optimal Möbius transformation. Landmarks are commonly used in brain mapping. We manually label the landmarks on the brain as a set of uniformly parametrized sulcal curves [8], as shown in Fig. 9. First we conformally map two brains to the sphere, then we pursue an optimal Möbius transformation to minimize the Euclidean distance between the corresponding landmarks on the spheres. Suppose the landmarks are represented as discrete point sets, and denoted as $\{p_i \in S_1\}$ and $\{q_i \in S_2\}, p_i$ matches $q_i, i = 1, 2, \ldots, n$. The landmark mismatch functional for $u \in \Omega$ is defined as

$$E(u) = \sum_{i=1}^{n} \left\| f_1^{-1}(p_i) - u\left(f_2^{-1}(q_i)\right)\right\|^2, \quad u \in \Omega, \quad p_i \in S_1, \quad q_i \in S_2. \tag{24}$$

In general, the above variational problem is a nonlinear one. In order to simplify it, we convert it to a least squares problem. First we project the sphere to the complex plane, then the Möbius transformation is represented as a complex linear rational formula, (17). We add another constraint for u, so that u maps infinity to infinity. That means the north poles of the spheres are mapped to each other. Then u can be represented as a linear form $az + b$. Then the functional of u can be simplified as

$$E(u) = \sum_{i=1}^{n} g(z_i)|az_i + b - \tau_i|^2 \tag{25}$$

where z_i is the stereo-projection of p_i, τ_i is the projection of q_i, g is the conformal factor from the plane to the sphere, which can be simplified as

$$g(z) = \frac{4}{1 + z\bar{z}}. \tag{26}$$

So the problem is a least squares problem.

VI. Spherical Harmonic Analysis

Let $L^2(S^2)$ denote the Hilbert space of square integrable functions on the S^2. In the spherical coordinates, θ is taken as the polar (colatitudinal) coordinate with $\theta \in [0, \pi]$, and ϕ as

the azimuthal (longitudinal) coordinate with $\phi \in [0, 2\pi)$. The usual inner product is given by

$$\langle f, h \rangle = \int_0^{\pi} \left[\int_0^{2\pi} f(\theta, \phi) \overline{h(\theta, \phi)} d\phi \right] \sin\theta \, d\theta. \tag{27}$$

A function $f : S^2 \to \mathbb{R}$ is called a *Spherical Harmonic*, if it is an eigenfunction of Laplace–Beltrami operator, namely $\Delta f = \lambda f$, where λ is a constant. There is a countable set of spherical harmonics which form an orthonormal basis for $L^2(S^2)$. For any nonnegative integer l and integer m with $|m| \leq l$, the (l, m)-spherical harmonic Y_l^m is a harmonic homogeneous polynomial of degree l. The harmonics of degree l span a subspace of $L^2(S^2)$ of dimension $2l + 1$ which is invariant under the rotations of the sphere. The expansion of any function $f \in L^2(S^2)$ in terms of spherical harmonics can be written

$$f = \sum_{l \geq 0} \sum_{|m| \leq l} \hat{f}(l, m) Y_l^m \tag{28}$$

and $\hat{f}(l, m)$ denotes the (l, m) *Fourier coefficient*, equal to $\langle f, Y_l^m \rangle$. Spherical harmonic Y_l^m has an explicit formula

$$Y_l^m(\theta, \phi) = k_{l,m} P_l^m(cos\theta) e^{im\phi} \tag{29}$$

where P_l^m is the *associated Legendre function* of degree l and order m, and $k_{l,m}$ is a normalization factor. The details are explained in [24].

Once the brain surface is conformally mapped to S^2, the surface can be represented as three spherical functions, $x^0(\theta, \phi), x^1(\theta, \phi)$, and $x^2(\theta, \phi)$. The function $x^i(\theta, \phi) \in L^2(S^2)$ is regularly sampled and transformed to $\hat{x^i}(l, m)$ using the fast spherical harmonic transformation as described in [25].

Many processing tasks that use the geometric surface of the brain can be accomplished in the frequency domain more efficiently, such as geometric compression, matching, surface denoising, feature detection, and shape analysis [26], [27].

A. Brain Geometry Compression

Similar to image compression using Fourier analysis, geometric brain data can be compressed using spherical harmonic analysis [26]. Global geometric information is concentrated in the low-frequency components, whereas noise and locally detailed information are concentrated in the high-frequency part. By using low-pass filtering, we can keep the major geometric features and compress the brain surface without losing too much information.

B. Rotation Invariant Shape Descriptor

The geometric representation $(x^1(\theta, \phi), x^2(\theta, \phi), x^3(\theta, \phi))$ depends on the orientation of the brain. Brain registration has to be applied first in order to compare the geometric representations of two different brains. A rotation-invariant shape descriptor can be formulated based on the frequency coefficients. Because the harmonics of degree l span the rotation invariant subspace of $L^2(S^2)$, the following shape descriptor is also rotation invariant:

$$s(l) = \sum_i \sum_{|m| \leq l} ||\hat{x}^i(l, m)||^2. \tag{30}$$

TABLE II
CPU TIMES FOR SURFACES OF DIFFERENT TRIANGLE COUNT ON A 1.9-GHZ PC WITH WINDOWS XP OPERATING SYSTEM

# of vertices	# of faces	time (sec)
5002	10000	145
10002	20000	372
15002	30000	540

Given two brain surfaces, we can compute their shape descriptor from their spherical harmonic spectrum, and compare them directly without any registration.

Fig. 12 illustrate the shape descriptors for the same brain with different orientations. It is clear that the shape descriptor is totally rotation invariant [28].

The brain surface can be represented as a vector valued function defined on the sphere via conformal mapping of its surface to the surface. The brain surface can then be decomposed in terms of linear combination of spherical harmonics. The vector valued spectrum, i.e., the harmonic coefficients expressed as components of a vector, can be used to analyze the shape. The main geometric features are encoded in the low-frequency part, while the noise will be in the high-frequency part. By filtering out the high-frequency coefficients, we can smooth the surface, and compress the geometry. By comparing the low-frequency coefficients, we can match surfaces, and compute the similarity of surfaces.

VII. EXPERIMENTAL RESULTS

The algorithm uses covariant differentiation to solve a geometric nonlinear partial differential equation (PDE). The complexity of the algorithm is $O(mn)$, where m is the number of the vertices of the brain mesh, n is the number of required iterations. n mainly depends on the initial condition, i.e., how close it is to a conformal map. n also depends on the step length. Table II illustrates the CPU time for computing conformal maps of surfaces of different triangle numbers on a 1.9-GHz PC with the Windows XP operating system.

Comparing to other algorithms that solve a linear system, such as Haker *et al.* [6], our nonlinear algorithm has the following unique advantages. First, every point on the brain is treated in a uniform way—no point maps to infinity as in [6]. Therefore, there are no specific areas with large distortion. Second, the method is very general, as it does not require the target surface to be a sphere. It can be easily generalized to compute harmonic maps between any two arbitrary genus zero surfaces.

The 3-D brain meshes are reconstructed from 3-D $256 \times 256 \times 124$ T1 weighted SPGR (spoiled gradient) MRI images, by using an active surface algorithm that deforms a triangulated mesh onto the brain surface [9]. Fig. 5(a) and (c) shows the same brain scanned at different times [8]. Because of the inaccuracy introduced by scanner noise in the input data, as well as slight biological changes over time, the geometric information is not exactly the same. Fig. 5(a) and (c) reveals minor differences.

The conformal mapping results are shown in Fig. 5(b) and (d). From this example, we can see that although the brain meshes are slightly different, the mapping results look quite similar. The

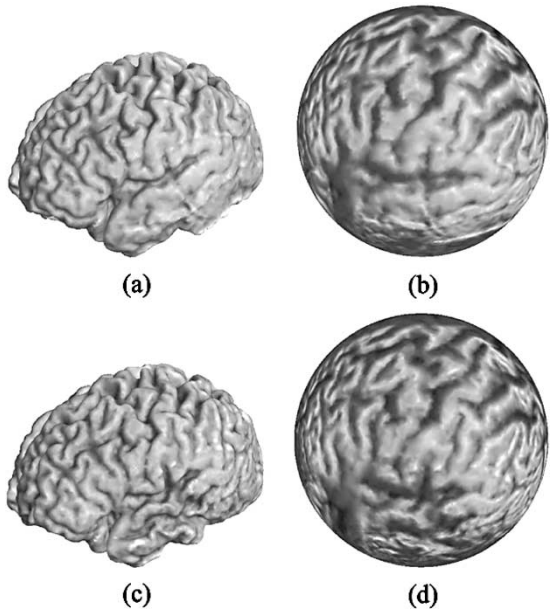

Fig. 5. Reconstructed brain meshes and their spherical harmonic mappings. (a) and (c) are the reconstructed surfaces for the same brain scanned at different times. Due to scanner noise and inaccuracy in the reconstruction algorithm, there are visible geometric differences. (b) and (d) are the spherical conformal mappings of (a) and (c), respectively; the normal information is preserved. By the shading information, the correspondence is illustrated.

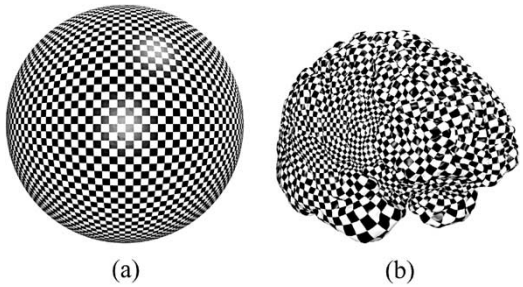

Fig. 6. Conformal texture mapping. (a) Texture mapping of the sphere; (b) Texture mapping of the brain. The conformality is visualized by texture mapping of a checkerboard image. The sphere is mapped to the plane by stereographic projection, then the planar coordinates are used as the texture coordinates. This texture parameter is assigned to the brain surface through the conformal mapping between the sphere and the brain surface. All the right angles in the texture are preserved on the brain surface.

major features are mapped to the same position on the sphere. This suggests that the computed conformal mappings continuously depend on the geometry, and can match the major features consistently and reproducibly. In other words, conformal mapping may be a good candidate for a canonical parameterization in brain mapping.

Fig. 6 shows that the mapping is conformal by texture mapping a checkerboard to both the brain surface mesh and a spherical mesh. Each black or white square in the texture is mapped to sphere by stereographic projection, and pulled back to the brain. Note that the right angles are preserved both on the sphere and the brain.

Comparing conformal mapping to other spherical mapping method, such as Tuette brain mapping, the major difference is that Tuette is not intrinsic, and it highly depends on the representation of the surface, including the triangulation and resolution.

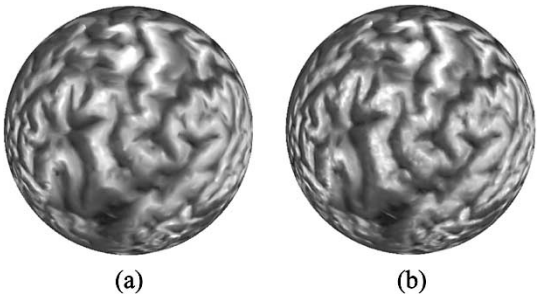

Fig. 7. Conformal mappings of surfaces with different resolutions. (a) Surface with 20 000 faces; (b) Surface with 50 000 faces. The original brain surface has 50 000 faces, and is conformally mapped to a sphere, as shown in (a). Then, the brain surface is simplified to 20 000 faces, and its spherical conformal mapping is shown in (b).

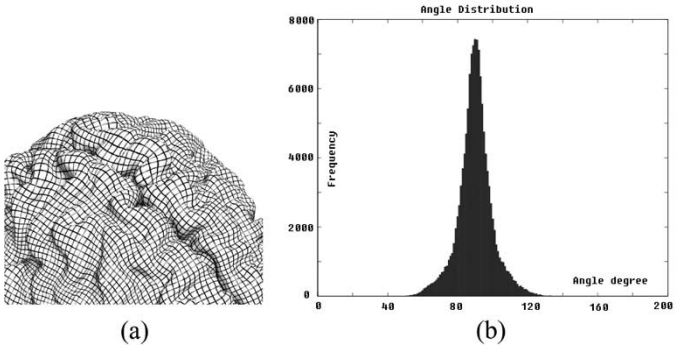

Fig. 8. Conformality measurement. (a) Intersection angles; (b) Angle distribution. The curves of iso-polar angle and iso-azimuthal angle are mapped to the brain, and the intersection angles are measured on the brain. The histogram is illustrated.

Even for the same brain, different representations will produce different mapping results. Conformal mapping is more valuable for practical purposes. Conformal mappings are stable and depend continuously on the input geometry but not on the triangulations, and are insensitive to the resolutions of the data. Fig. 7 shows the same surface with different resolutions, and their conformal mappings. The mesh simplification is performed using a standard method. The refined model has 50 k faces, but the coarse one has 20 k faces. The conformal mappings map the major features to the same positions on the spheres.

In order to measure the conformality, we map the iso-polar angle curves and iso-azimuthal angle curves from the sphere to the brain by the inverse conformal mapping, and measure the intersection angles on the brain. The distribution of the angles of a subject (A) are illustrated in Fig. 8. The angles are concentrated about the right angle.

Fig. 9 shows the landmarks, and the result of the optimization by a Möbius transformation. Our landmarks consist of a set of sulcal lines that were manually traced on 3-D surface models extracted from individual MRI images [29]. The lines correspond to various sulci, such as the central sulcus, post-central sulcus, pre-central sulcus, etc. The mappings were constrained by all landmarks that occur consistently in the brains being matched.

We also computed the matching energy, following (22). We did our testing on three example subjects. Their information is shown in Table III. We took subject A as the target brain.

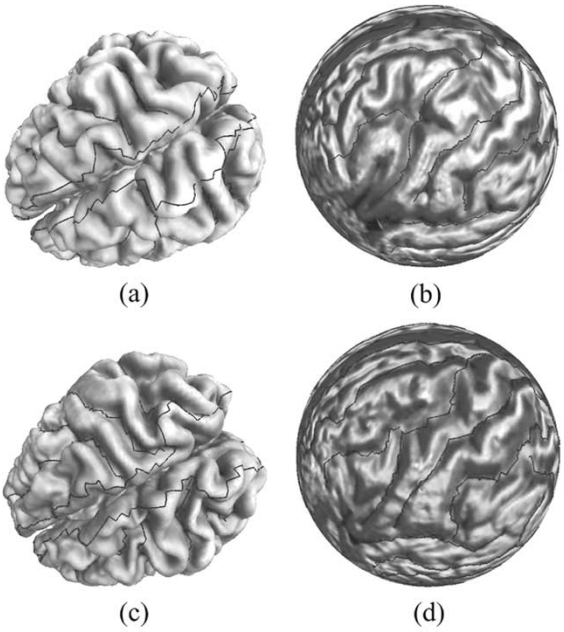

Fig. 9. Möbius transformation to minimize the deviations between landmarks. The dark curves are the landmarks. The correspondence between curves has been preassigned. The desired Möbius transformation is obtained to minimize the matching error on the sphere.

TABLE III
MATCHING ENERGY FOR THREE SUBJECTS. SUBJECT A WAS USED AS THE TARGET BRAIN. FOR SUBJECTS B AND C, WE FOUND MÖBIUS TRANSFORMATIONS THAT MINIMIZED THE LANDMARK MISMATCH FUNCTIONS, RESPECTIVELY

Subject	Vertex #	Face #	Before	After
A	65,538	131,072	-	-
B	65,538	131,072	604.134	506.665
C	65,538	131,072	414.803	365.325

For each new subject model, we found a Möbius transformation that minimized the landmark mismatch energy on the maximum intersection subsets of it and A. As shown in Table III, the matching energies were reduced after the Möbius transformation.

Fig. 10 illustrates the geometric compression results using spherical harmonic compression. Fig. 11 shows the L^2 errors of the compression result. The low-pass filters are applied to remove high-frequency components, and the surfaces are reconstructed from the remaining low-frequency components. The surface is normalized such that the total area is 4π, then the L^2 error between the reconstructed surface and the original surface is computed. The curve shows the normalized L^2 error vs the ratio of retained low-frequency components. The figure illustrates that the major geometric information is encoded in the low-frequency part.

Fig. 12 illustrates the relative error between the rotation-invariant shape descriptors for the original brain surface and for the rotated brain surface. Because the first 30 low-frequency components generate more than 99% of the total energy, only the first 30 shape descriptor errors are shown in the figure. From the figure, it is clear that the relative errors are less than 1% and, therefore, the shape descriptors are rotation invariant.

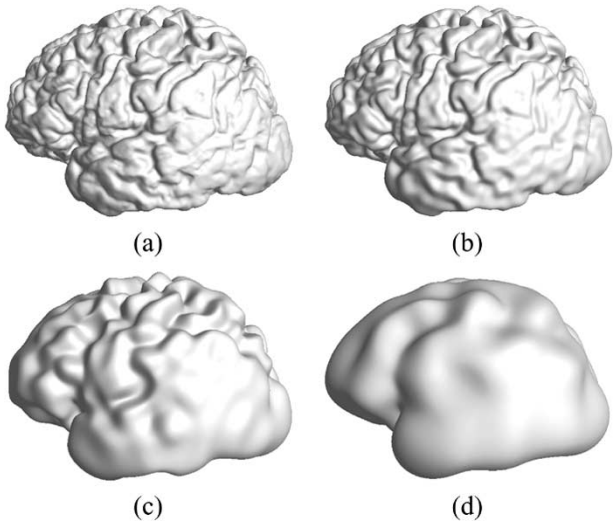

Fig. 10. This figure illustrates the geometric compression results using spherical harmonics. After we conformally map the brain to a sphere, we can use spherical harmonics to compress the geometry. (a) is the original brain surface. (b), (c), and (d) are brain surfaces reconstructed from spherical harmonics with $(1/8), (1/64)$, and $(1/256)$ of the original low-frequency coefficients, separately.

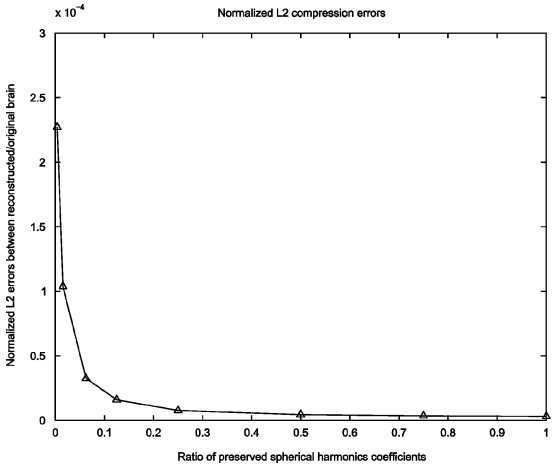

Fig. 11. This figure illustrates the normalized L^2 errors of the compression.

The method described in this paper is quite general. We tested the algorithm on other genus zero surfaces, including the hand and foot surface. Some of the experimental results are illustrated in Fig. 13.

VIII. COMPARISON WITH OTHER WORK

Several other studies of conformal mappings between brain surfaces are reported in [5], [6], [17], and [19]. In [5] and [19], Hurdal *et al.* used the circle packing theorem and the ring lemma to establish a theorem: there is a unique circle packing in the plane (up to certain transformations) which is quasi-conformal (i.e., angular distortion is bounded) for a simply-connected triangulated surface. They demonstrated their experimental results for the surface of the cerebellum. This method only considers the topology without considering the brain's geometric structure. Given two different mesh structures of the same brain, one can predict that their methods may generate two different mapping results. Compared with their work, our method preserves

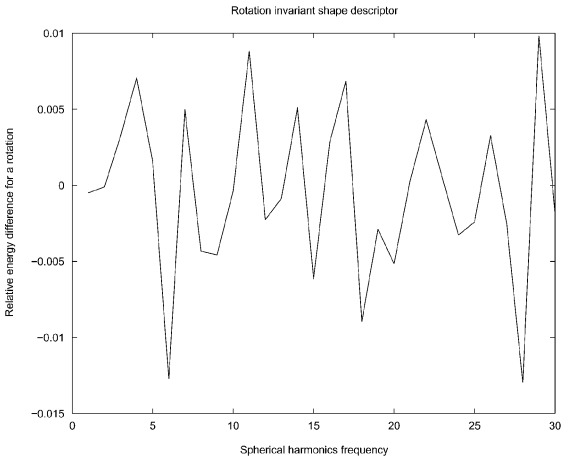

Fig. 12. The brain surface is rotated 90 degree with respect to x-axis. The shape descriptors defined in (30) are computed for both the original surface and the rotated surface, denoted as $s(l)$ and $s'(l)$, respectively. The relative errors $(s(l) - s'(l))/s(l)$ are illustrated as a function of l. Because the first $30s(l)$ generate almost all the energy, the curve is truncated at $l = 30$. From the curve it can be verified that the relative error is less than 1%, and, thus, the shape descriptors are rotation invariant.

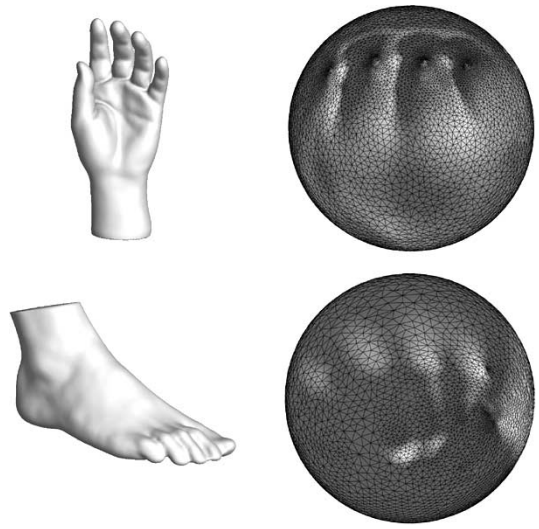

Fig. 13. Spherical conformal mapping of genus zero surfaces. Extruding parts (such as fingers and toes) are mapped to denser regions on the sphere.

angles and establishes a good mapping between brains and a canonical space.

Haker *et al.* [6], [17] built a finite element approximation of the conformal mapping method for brain surface parameterization. They selected a point as the north pole and conformally mapped the cortical surface to the complex plane. In the resulting mapping, the local shape is preserved and distances and areas are only changed by a scaling factor. Based on Haker *et al.* [6], Joshi *et al.* [30] obtained a unique conformal mapping by fixing three point correspondences between two brains. Since stereo projection is involved, there is significant distortion around the north pole areas, which brings instability to this approach. Compared with their work, our method is more accurate, with no regions of large area distortion. It is also more stable and can be readily extended to compute maps between two general manifolds.

Finally, we note that Memoli *et al.* [31] mentioned they were developing implicit methods to compute harmonic maps between general source and target manifolds. They used level sets to represent the brain surfaces. Due to the extensive folding of the human brain surface, these mappings have to be designed very carefully.

IX. Conclusion and Future Work

In this paper, we apply part of the algorithms [1], [2] (for genus zero surface) to the cortical surface matching problem. The algorithm finds a unique conformal mapping between genus zero manifolds. Our method only depends on the surface geometry and not on the mesh structure (i.e., gridding) and resolution. Our algorithm is very fast and stable in reaching a solution. There are numerous applications of these mapping algorithms, such as providing a canonical space for automated feature identification, brain to brain registration, brain structure segmentation, brain surface denoising, shape analysis and convenient surface visualization, among others. We are trying to generalize this approach to compute conformal mappings between nonzero genus surfaces.

Acknowledgment

The 3-D model of Head of Michelangelo's David is courtesy of the Digital Michelangelo Project 3D Model Repository. The authors thank anonymous referees for their helpful suggestions.

References

[1] X. Gu and S. Yau, "Computing conformal structures of surfaces," *Commun. Inform. Syst.*, vol. 2, no. 2, pp. 121–146, Dec. 2002.
[2] ——, "Global conformal surface parameterization," in *Proc. ACM Symp. Geometry Processing*, 2003, pp. 127–137.
[3] E. Schwartz, A. Shaw, and E. Wolfson, "A numerical solution to the generalized mapmaker's problem: Flattening nonconvex polyhedral surfaces," *IEEE Trans. Pattern Anal. Machine Intell.*, vol. 11, pp. 1005–1008, Sept. 1989.
[4] B. Fischl, M. Sereno, R. Tootell, and A. Dale, "High-resolution intersubject averaging and a coordinate system for the cortical surface," *Hum. Brain Mapp.*, vol. 8, pp. 272–284, 1999.
[5] M. Hurdal, K. Stephenson, P. Bowers, D. Sumners, and D. Rottenberg, "Coordinate systems for conformal cerebellar flat maps," *NeuroImage*, vol. 11, p. S467, 2000.
[6] S. Haker, S. Angenent, A. Tannenbaum, R. Kikinis, G. Sapiro, and M. Halle, "Conformal surface parameterization for texture mapping," *IEEE Trans. Visual. Comput. Graphics*, vol. 6, pp. 181–189, Apr.–June 2000.
[7] B. Timsari and R. Leahy, "An optimization method for creating semi-isometric flat maps of the cerebral cortex," *Proc. SPIE (Medical Imaging)*, Feb. 2000.
[8] P. Thompson, M. Mega, C. Vidal, J. Rapoport, and A. Toga, "Detecting disease-specific patterns of brain structure using cortical pattern matching and a population-based probabilistic brain atlas," in *Proc. 17th Int. Conf. Information Processing in Medical Imaging (IPMI2001)*, Davis, CA, June 18–22, 2001, pp. 488–501.
[9] P. Thompson and A. Toga, "A framework for computational anatomy," in *Comput. Visual. Sci.*, vol. 5, 2002, pp. 1–12.
[10] R. Schoen and S. Yau, *Lectures on Harmonic Maps*. Cambridge, MA: Harvard Univ., Int. Press, 1997.
[11] M. Eck, T. DeRose, T. Duchamp, H. Hoppe, M. Lounsbery, and W. Stuetzle, "Multiresolution analysis of arbitrary meshes," *Comput. Graphics (Proc. SIGGRAPH 95)*, Aug. 1995.
[12] P. Alliez, M. Meyer, and M. Desbrun, "Interactive geometry remeshing," *Comput. Graphics (Proc. SIGGRAPH 02)*, pp. 347–354, 2002.
[13] M. Desbrun, M. Meyer, and P. Alliez, "Intrinsic parametrizations of surface meshes," in *Proc. Eurographics*, 2002, pp. 210–218.
[14] U. Pinkall and K. Polthier, "Computing discrete minimal surfaces and their conjugates," *Exp. Math.*, vol. 2, no. 1, pp. 15–36, 1993.

[15] T. Kanai, H. Suzuki, and F. Kimura, "Three-dimensional geometric metamorphosis based on harmonic maps," *Visual Comput*, vol. 14, no. 4, pp. 166–176, 1998.

[16] B. Levy, S. Petitjean, N. Ray, and J. Maillot, "Least squares conformal maps for automatic texture atlas generation," *Comput. Graphics (Proc. SIGGRAPH 02)*, 2002.

[17] S. Angenent, S. Haker, A. Tannenbaum, and R. Kikinis, "Conformal geometry and brain flattening," in *Proc. MICCAI*, 1999, pp. 271–278.

[18] A. Sheffer and E. de Sturler, "Parameterization of faceted surfaces for meshing using angle-based flattening," *Eng. with Comput.*, vol. 17, pp. 326–337, 2001.

[19] M. Hurdal, P. Bowers, K. Stephenson, D. Sumners, K. Rehm, K. Schaper, and D. Rottenberg, "Quasiconformally flat mapping the human cerebellum," in *Lecture Notes in Computer Science*. Berlin, Germany: Springer-Verlag, 1999, vol. 1679, Proc. MICCAI'99, pp. 279–286.

[20] S. Haker, S. Angenent, A. Tannenbaum, and R. Kikinis, "Nondistorting flattening maps and the 3-d visualization of colon CT images," *IEEE Trans. Med. Imag.*, vol. 19, pp. 665–670, July 2000.

[21] K. Stephenson, "Approximation of conformal structures via circle packing," in *Computational Methods and Function Theory 1997, Proceedings of the Third CMFT Conference*. Singapore: World Scientific, 1999, pp. 551–582.

[22] D. Tosun and J. Prince, "Hemispherical map for the human brain cortex," *Proc. SPIE (Medical Imaging)*, p. **<Au: Page range?>**, Feb. 2001.

[23] D. Tosun, M. Rettmann, and J. Prince, "Mapping techniques for aligning sulci across multiple brains," presented at the *6th Annu. Int. Conf. Medical Image Computing and Computer-Assisted Interventions (MICCAI)*, Montréal, QC, Canada, Nov. 2003.

[24] N. Vilenkin, *Special Functions and the Theory of Group Representations*. Providence, RI: Amer. Math. Soc., 1968.

[25] D. Healy, D. Rockmore, P. Kostelec, and S. Moore, "Ffts for the 2-sphere—Improvements and variations," *J. Fourier Anal. Applicat.*, vol. 9, no. 4, pp. 341–385, 2003.

[26] C. Brechbühler, G. Gerig, and O. Kübler, "Surface parametrization and shape description," *Proc. SPIE (Visualization Biomed. Comp. 1992)*, vol. 1808, pp. 80–89, 1992.

[27] S. Joshi, U. Grenander, and M. Miller, "On the geometry and shape of brain sub-manifolds," *Int. J. Pattern Recogn. Artif. Intell. (Special Issue on Processing of MR Images of the Human)*, vol. 11, no. 8, pp. 1317–1343, 1997.

[28] G. Gerig, M. Styner, D. Jones, D. Weinberger, and J. Lieberman, "Shape analysis of brain ventricles using spharm," presented at the *IEEE Workshop on Mathematical Methods in Biomedical Image Analysis (MMBIA'01)*, Kauai, HI, Dec. 2001.

[29] P. Thompson, K. Hayashi, G. de Zubicaray, A. Janke, S. Rose, J. Semple, D. Herman, M. Hong, S. Dittmer, D. Doddrell, and A. Toga, "Dynamics of gray matter loss in alzheimer's disease," *J. Neurosci.*, vol. 23, no. 3, pp. 994–1005, 2003.

[30] A. Joshi and R. Leahy, "Invariant conformal mapping of cortical surfaces," in *Image analysis and understanding data from scientific experiments*. Los Alamos, NM: Los Alamos National Laboratory, Dec. 2002.

[31] F. Memoli, G. Sapiro, and S. Osher, "Solving Variational Problems and Partial Equations Mapping into General Target Manifolds," UCLA CAM, Tech. Rep. 02-04, Jan. 2002.

[32] X. Gu, Y. Wang, T. Chan, P. Thompson, and S.-T. Yau, "Genus zero surface conformal mapping and its application to brain surface mapping," in *Lecture Notes in Computer Science*, C. Taylor and J. Noble, Eds, Ambleside, UK: Springer-Verlag, July 2003, vol. 2732, Proc. 18th Int. Conf. Information Processing in Medical Imaging, pp. 172–184.